

Development of hybrid photonic integrated wavelength-tunable laser at 2 μm and its application to FMCW LiDAR

SANGHOON CHIN,^{1,*} JANNIS HOLZER,¹ ANDREAS DE GROOTE,²
DAAN MARTENS,² GRETA NAUJOKAITE,³ AUGUSTINAS
VIZBARAS,³  KRISTIJONAS VIZBARAS,³ AND CHRISTOPHE PACHE¹

¹Centre Suisse d'Electronique et de Microtechnique SA (CSEM), CH-2002 Neuchâtel, Switzerland

²Brolis Sensor Technology B.V., Bollebergen 2B Box 11, 9052, Zwijnaarde, Belgium

³Brolis Sensor Technology, UAB Moletu pl.73, LT-14259, Vilnius, Lithuania

*sanghoon.chin@csem.ch

Abstract: This paper reports on the experimental demonstration of a fully integrated frequency-modulated continuous-wave (FMCW) LiDAR sensing system, operating at 2.0 μm . It makes use of a widely tunable hybrid external cavity laser based on the combination of GaSb gain chip and silicon waveguide circuits. The single-frequency laser operation over the full spectral bandwidth of the gain chip is secured using a frequency-selective filter, consisting of two sequential microring resonators in a Vernier configuration. To increase the mode-hop free wavelength tuning range while preserving the linewidth of the laser, the heater of the phase section placed along the bus waveguide is synchronously controlled with two independent heaters placed on each microring resonator. This laser is then implemented for the development of an FMCW LiDAR, consisting of all-optical fiber-based two independent unbalanced Mach-Zehnder interferometers: k-space interferometer for the linearization of continuously swept laser frequency and main interferometer for the measurement of the distributed back-reflection over the distance. The optical frequency of the laser is continuously swept over a ~ 100 GHz range (or $\Delta\lambda=1.47$ nm at the operating wavelength) at a modulation speed of 100 Hz. Using this wavelength tunable laser, a light detection and ranging system (LiDAR) is experimentally demonstrated, showing a very high axial resolution of 1.36 mm in air with an extremely high precision of ~ 9 μm at a 100 Hz measurement rate.

© 2024 Optica Publishing Group under the terms of the [Optica Open Access Publishing Agreement](#)

1. Introduction

Over the last decade, the development of Light Detection and Ranging (LiDAR) as a range measurement sensing system has been extensively investigated since LiDAR systems have found tremendous applications in various domains such as 3-dimensional topology for geographically interesting terrains [1], atmospheric metrology [2], geochemical survey [3], robotics [4], space applications [5], just to mention a few. Especially, a remarkable market of LiDAR sensing systems is found in the automotive industry to support the development of advanced driver-assistance systems, and its market has significantly grown in recent years [6]. However, it must be noted that the most promising applications demand LiDARs with specific requirements, including being very compact in size, low power consumption, and cost-effectiveness. This is because the applications mentioned above essentially require multiple sensors to acquire a great amount of information at high speed. These days, it is widely acknowledged that photonic integrated circuit (PIC)-based LiDAR is the only technology capable of meeting these strict requirements. Many different material platforms such as silicon, silicon-nitride, and various III-V semiconductor materials have been already utilized to realize chip-scale LiDAR sensors [7–17].

To date, LiDAR sensing systems have been developed in two different architectures: pulsed time-of-flight (ToF) with a single-photon avalanched photodiode or frequency-modulated continuous-wave (FMCW) with a coherent detection. Since ToF-type LiDAR requires a high-power laser, resulting in a bulky sensor, the FMCW-type LiDAR, which operates at low laser power is considered a better practical solution for realizing chip-scale implementation. Moreover, the FMCW LiDAR has a few more inherent advantages such as cost-effective low bandwidth electronics for signal detection, reliable operation in daylight environments, and the simultaneous measurement of the range and velocity of target objects. To achieve the high performance of the FMCW LiDAR, it is necessary to employ a high coherent laser and a large mode-hop-free optical frequency tunability, which is the key to enabling long-range sensing and high precision of the distance ranging, respectively.

This paper presents, to the best of our knowledge, the first demonstration of an FMCW LiDAR sensing system operating at 2 μm , which makes use of an external cavity photonic-integrated wavelength-tunable laser engine. The main advantages of this wavelength, as opposed to the more commonly used 905 nm, lie in its eye-safety and a large potential for gas sensing and biomolecule monitoring, thanks to favorable absorption lines of various substances [18]. The laser engine is fabricated by the hybrid integration of a GaSb gain chip and a silicon photonics waveguide circuit to construct an external cavity for the wavelength section. A photodiode is also integrated on the same chip for the realization of a complete FMCW LiDAR transceiver, but for our demonstration experiment, an external photodetection system is utilized. A Vernier-type external cavity consisting of two cascaded microring resonators is integrated into the inherent laser cavity for the single-mode operation, and a phase section is also integrated into the laser cavity to control the optical phase of the recirculating light, which changes the laser frequency [19]. Overall, 3 phase controllers implemented for two microrings and phase section are independently and synchronously controlled to sweep the laser frequency in time, resulting in a continuous frequency sweep range of >100 GHz at 100 Hz frequency modulation speed. This way a high-performance FMCW LiDAR is successfully demonstrated, showing an axial resolution of 1.3 cm and ranging precision of 9.2 μm .

2. Development of a hybrid integrated laser with a large wavelength tunability

The wavelength tunable laser that is implemented to develop the proposed FMCW LiDAR sensing system at 2 microns is fabricated by Brolis Sensor Technology, using a hybrid GaSb/Si external cavity structure. Such configuration makes use of a GaSb platform type-I quantum well gain-chip with an angled waveguide and HR/AR coated facets. The spontaneous amplified emission generated from the gain chip is butt-coupled to a silicon-on-insulator (SOI) platform photonic integrated circuit (PIC) chip via a spot-size mode converter. Figure 1 illustrates the simplified schematic diagram of the hybrid tunable laser. On the PIC chip, various light manipulation circuits are integrated to provide emission wavelength tuning, optical feedback, optical phase shifter and light output coupler as well as monitoring ports for the output optical power and wavelength (not shown in Figure).

The main building blocks of the external cavity laser are the Vernier filter, realized using two independent micro-ring resonators and a distributed feedback Bragg reflector (DBR). The ring resonators has a slightly different radius of ~ 31.5 μm and ~ 29 μm , and the coupling gap between the rings and the bus waveguides is ~ 500 nm, resulting in a simulated coupling coefficient κ of around 0.06 at the wavelength of 2 μm . An additional phase control to enlarge the wavelength sweep range without mode-hop is achieved using a spiral waveguide index tuning. To continuously sweep the laser frequency, the optical properties of two μ -ring resonators and the spiral phase shifter are tuned independently using electro-thermal heaters by applying a voltage across the heater electrodes while the laser is stabilized in temperature and is driven at a fixed injection current. In this work, a standard 220 nm silicon waveguide on insulator PIC platform is

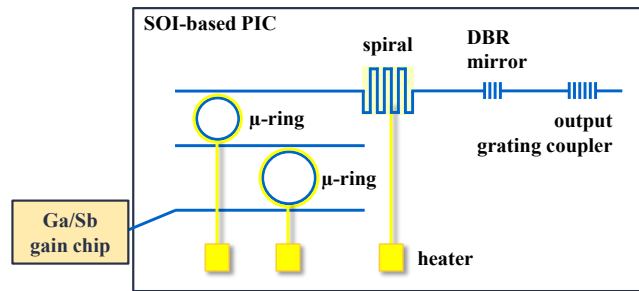


Fig. 1. Schematic diagram of the hybrid GaSb/Si external cavity tunable laser. SOI: silicon-on-insulator. DBR: distributed Bragg reflector

utilized. GaSb gain-chip is grown by the molecular beam epitaxy and processed into an angled ridge-waveguide device. The cavity length with a ridge width of 4 microns is designed to be 0.7 mm. The back-facet is coated with a high-reflectivity mirror ($R > 96\%$) whereas the front-facet has an ultra-low reflectivity coating with a modal power reflectivity of $< 0.1\%$. Moreover, the laser output from the external cavity laser is realized by means of a grating coupler. The light from the grating coupler is then collected with a polarization-maintaining single-mode fiber (PMF) for the LIDAR experiment. The linear polarization of the light emerging from the PIC laser is well aligned to the slow axis of the PMF using a fiber rotator for the bare fiber (HFR007, Thorlabs). Moreover, the base plate temperature of the integrated laser is effectively stabilized by a thermoelectric cooler (TEC) that is controlled via a PCB-based electronic driver, as shown in the block diagram in Fig. 2. An internal photodetector that is not depicted in the Figure is effectively used to monitor the continuity of the output power during the wavelength sweep since the presence of mode hops manifests abrupt changes in the intensity of the lasing mode.

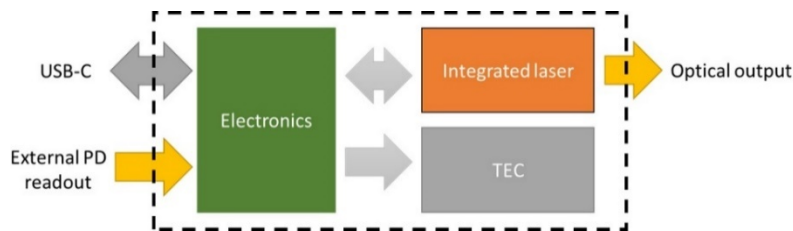


Fig. 2. Schematic diagram of the integrated laser unit for the experiment. PD: photodetector. TEC: thermoelectric cooler.

A 1m-long PMF (Nufern PM-1950) is used to couple the light exiting from the PIC chip to an optical fiber, resulting in ~ 100 μW optical power at the optical fiber while the polarization state of light is aligned to the slow axis of the PMF. However, it is worth noting that this level of laser power was sufficient to demonstrate the proof-of-concept LiDAR sensing system. Therefore, no further effort was made to investigate and improve the coupling efficiency. Then, the linewidth of the integrated laser operating under steady-state conditions was unambiguously measured by using the delayed self-homodyne method [20], which makes use of an unbalanced Mach-Zehnder interferometer, as shown in Fig. 3(a). A 650 m-long standard single-mode fiber as an optical delay-line was placed in the bottom arm of the interferometer to introduce a random differential optical phase between the two arms. In consequence, the light from the two arms turns to be totally incoherent to each other. Therefore, when they recombine at the output of the interferometer their mutual interference leads to an electrical beat signal, whose spectral profile essentially represents the auto-cross correlation of the power spectrum of the incident light. Since the

measured spectrum of the electrical beat signal shows a good agreement with a Gaussian-shaped field spectrum, the linewidth of the laser was interpreted to be 12.3 MHz at the full width at half maximum (FWHM) under the estimation of Gaussian optical lineshape, as shown in Fig. 3(b). In fact, the dynamic linewidth of the laser is more relevant to the FMCW LiDAR performance since the laser frequency is continuously swept in time. In this work we tested the frequency sweeping speed up to 5 kHz and focused on 100 Hz for the sensor performance evaluation. For this reason, the delayed-heterodyne beat signal is measured by an electrical spectrum analyzer with a spectral resolution of 10 Hz and video resolution of 100 Hz to appropriately estimate the averaged linewidth of the laser over 10 ms. The relatively large laser linewidth might be attributed to two main factors. Firstly, the Q factor of the Vernier filter is expected to be relatively low to facilitate an ultimate bandwidth of wavelength tuning range since the PIC used in this work is designed to develop widely wavelength-tunable laser. The second reason may rely on the relatively low optical coupling efficiency between GaSb gain-chip and SOI-based PIC, which is still related to the Q factor of the cavity.

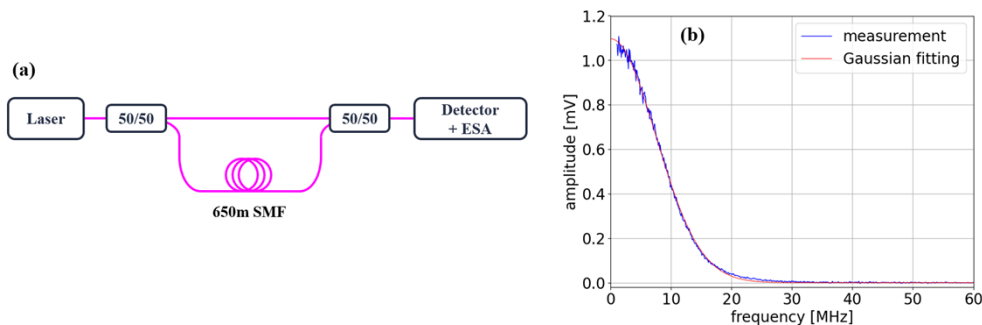


Fig. 3. (a) Simplified schematic diagram of laser linewidth measurement setup, based on delayed self-homodyne method. (b) Electrical spectrum of the beat signal, resulting in the laser FWHM linewidth of 12.3 MHz under the estimation of Gaussian optical lineshape. SMF: single-mode fiber. ESA: electrical spectrum analyzer.

The dynamic linewidth of the laser under operating conditions of fast optical frequency sweep was further investigated since the ambiguity range of the FMCW LiDAR is effectively limited by the dynamic laser linewidth rather than the static linewidth. The optical setup to evaluate the dynamic laser linewidth is illustrated in Fig. 4(a). The frequency-swept laser is split into two branches and half of the light is sent to the k -space interferometer to measure the instantaneous optical frequency of the laser. More details on the k -space analysis will be discussed in Section §3. The other arm is directed to the optical fiber ring cavity, constructed by using a directional coupler [21]. Under specific conditions of our experimental setup: the optical power split ratio of 95.2% and 4.8% and the ring cavity length of 37.5 cm with the refractive index of $n = 1.447$, the free spectral range (FSR) of the ring cavity is theoretically calculated to be 552.9 MHz. However, due to the undesirable large intrinsic insertion loss of 1.65 dB through the coupler that is inevitably caused by a large material absorption at 2 microns, the spectral broadening of the optical resonance to 69.3 MHz is expected at the output of the ring cavity.

Figure 4(b) demonstrates measured spectral profiles of the transmission through the cavity at 4 different frequency sweep speeds: 1, 10, 100 and 5000 Hz. Since the spectral profile of the measured transmission is expressed by the convolution between two spectra of the ring cavity resonance and interrogating light source with Gaussian line shape, the effective spectral width of the transmission through the cavity was measured to be 76.9 MHz that is the averaged width over the 4 transmission spectra, showing a good agreement to the theoretical spectral width of 77.7 MHz. As a result, it can be deduced that the dynamic linewidth of the frequency-swept

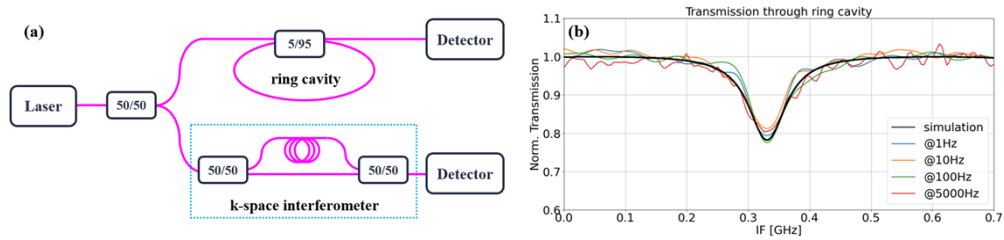


Fig. 4. (a) Simplified schematic diagram to characterize the dynamic laser linewidth under operation conditions of fast optical frequency sweep. (b) Comparison between calculated and measured transmission profile through a fiber ring resonator with FSR of 500 MHz with FWHM linewidth of 5 MHz at different frequency sweep speeds.

laser seems to be not influenced by the modulation speed, at least up to 5 kHz. In other words, it proves the time synchronization between the three individual heaters integrated on the two microring resonators and the phase section, since the linewidth of the laser is severely subject to the spectral bandwidth of the Vernier filter.

3. Experimental result on high-resolution FMCW LiDAR

Figure 5 illustrates the simplified schematic diagram of the FMCW LiDAR that we developed, using the hybrid photonic integrated wavelength-tunable laser at 2 microns. The sensing system consists mainly of two independent Mach-Zehnder interferometers (MZI), namely the k-space interferometer and the main interferometer, respectively. The two interferometers are constructed by polarization-maintaining fibers (PMF) to avoid any adverse polarization fading effects in the detection system. The primary role of the k-space MZI is to eliminate the detrimental nonlinearity that is imposed along the continuous optical frequency sweep; hence, improving the axial resolution and accuracy of the distance ranging in the sensing system [22]. A fixed optical delay line, which is a ~ 10 cm-long optical fiber in our experiment, is placed in the upper arm of the k-space MZI. Such an unbalanced MZI acts as a periodic spectral filter, whose free spectral range (FSR) is expressed as $c/(n_g \cdot \Delta L)$, where c is the light speed in vacuum, n_g is the refractive group index of the optical fiber, ΔL is the physical path length difference. In turn, the FSR was accurately measured by scanning the optical frequency of a commercial DFB laser (Eblana Photonics) operating at 2004 nm that has a current-wavelength tuning coefficient of 2.98 pm/mA, equivalent to 2.23 GHz/mA. The laser output is directly sent to the k-space interferometer and the transmission at the interferometer output is measured as a function of the injection current from 50 mA to 110 mA by 1 mA step, resulting in the FSR of 2.065 GHz, which matches well the theoretical value calculated by the unbalanced physical length of the MZI and the refractive index of the optical fiber.

When continuously frequency-swept light is sent to the k-space interferometer, the interference signal at the interferometer output, referred to as interferogram, has a sinusoidal waveform. Therefore, the instantaneous optical frequency of the frequency-swept laser can be mathematically retrieved by extracting the phase information of the measured sinusoidal waveform. In fact, the temporal variation of the phase of the signal is precisely obtained by performing the Hilbert transformation of the measured interferogram, at which a phase change of 2π corresponds to the optical frequency change of the FSR of the unbalanced MZI. It is also important to mention that any presence of mode hop behavior during the frequency sweep will induce abrupt discrepancies in the retrieved time-varying phase profile. For this reason, the Hilbert transform compensation method (HTCM) [22,23] is most widely used to evaluate the continuity of frequency-swept light sources. Moreover, such a process of the linearization of continuous optical frequency

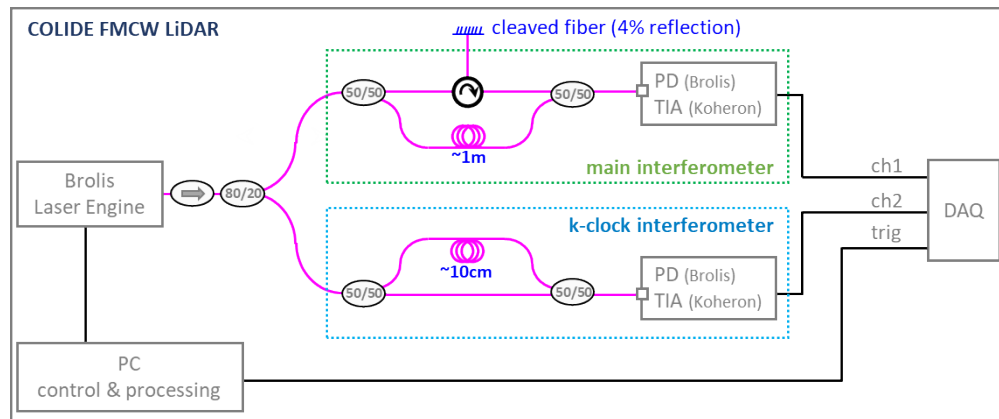


Fig. 5. Simplified schematic diagram of FMCW LiDAR at $2\ \mu\text{m}$, using the hybrid integrated wavelength tunable laser.

sweep is essential to secure the performance of an FMCW LiDAR sensing system, especially in terms of axial resolution in ranging and sensing sensitivity. Figure 6(a) illustrates an exemplary interferogram obtained from the k-space interferometer while the laser frequency was continuously swept at 10 Hz. As expected, the measured interferogram exhibits a smooth sinusoidal waveform, but the nonlinear chirp behavior is clearly seen along the waveform. Such nonlinear frequency sweep behavior is analyzed quantitatively by the HTCMT, as shown in Fig. 6(b). The measured interferogram is then projected in the optical frequency domain, simply by replacing the time axis of the interferogram with the retrieved instantaneous optical frequency. This way the inevitable nonlinearity imposed on the measured interferogram in the time domain is effectively eliminated, resulting in the linear interferogram in the optical frequency domain. Therefore, after resampling the interferogram with an equidistant optical frequency grid, the reflection profile of the FMCW LiDAR is essentially obtained in the time domain by performing the Fourier transformation of the resampled interferogram, as shown in Fig. 6(c), at which the distance is obtained by multiplying the retrieved time by the speed of light in air.

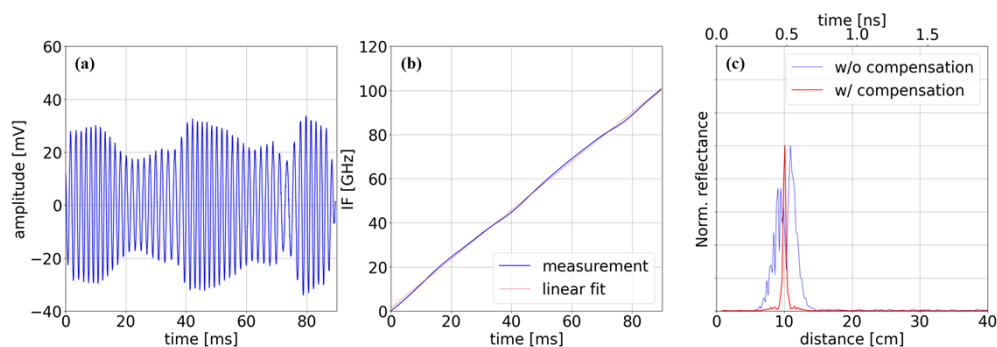


Fig. 6. (a) Measured interference signal at the k-space interferometer output. (b) Retrieved instantaneous optical frequency over time, clearly showing nonlinear components during the continuous frequency sweep. (c) Measured reflection profile by the FMCW LiDAR with and without the compensation of nonlinearity in the frequency sweep.

The characteristics of the continuous optical frequency sweep of our laser are evaluated for different modulation speeds at 1, 10, 100, 1000 and 5000 Hz, as shown in Fig. 7(a), at which

the time axis is normalized to 1 for the clear comparison purpose between different modulation speeds. As clearly seen, the behavior of nonlinear frequency sweep is present for all modulation speeds, and the degree of the nonlinearity tends to be larger for higher modulation speeds. Nevertheless, the optical frequency sweep without mode-hop is successfully achieved for all modulation speeds, resulting in the continuous optical frequency sweeping range of 111 GHz and 95 GHz for the modulation speed of 1 Hz and 5 kHz, respectively. As seen in Fig. 7(b), the amount of the measured frequency sweep is reduced as the sweep speed increases, which is essentially attributed to the slow thermal response time of the laser cavity.

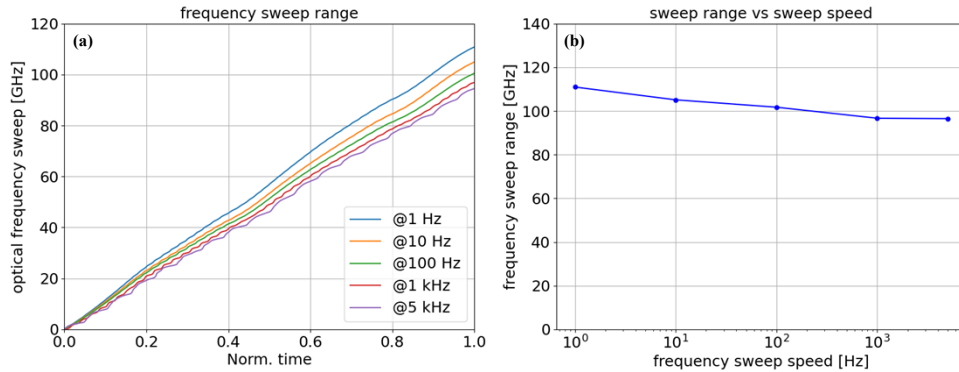


Fig. 7. Measured optical frequency sweep range as a function of frequency sweep speed.

To evaluate the ranging performance of the FMCW LiDAR sensing system, a part of the frequency-swept laser is delivered to the main MZ interferometer (See Fig. 5), at which the FMCW light is split into two branches. The light through one branch is directly sent to the photodetector to play the role of local oscillator while the light through the other branch is employed to illuminate a sample under test after passing through an optical circulator. The back-reflection from the sample returns to the sensing system, and then is combined with the local oscillator. As a result of the mutual interference, a beat signal referred to as an interferogram is generated and is recorded by a data acquisition card (ACQ2000X_OCTOPUS, ACQUITEK). Notice that the signal from the k-space interferometer is also simultaneously acquired to eliminate the nonlinearity that is essentially imposed onto the interferogram obtained from the main interferometer.

Our frequency-swept laser is operated at 100 Hz with a frequency sweep range of 102 GHz, which is equivalent to the axial resolution of 1.4 cm in distance ranging. As for the sensing sample under test, a polarization-maintaining optical fiber, 40 cm in length with a flat-cleaved end, is connected to the circulator. Thereby, when the laser strikes the interface between the optical fiber and the ambient air, we expect that 3.3% of Fresnel back-reflection is generated from the interface, which combines with the local oscillator at the photodetector, resulting in an interferogram. This interferogram obtained from the main interferometer is processed in the same manner as explained above. Figure 8(a) depicts the measured reflection profile, showing a sharp reflection peak at 40 cm, corresponding to the sample fiber length. On the other hand, the inset in the Figure shows the magnification of the reflection peak in distance, and the full width at half maximum of the resonance, which is the definition of the axial resolution of FMCW LiDAR, is measured to be 1.3 cm, showing a good agreement with the expected value as estimated above. Furthermore, the ranging measurement is continuously performed to evaluate the precision of the range sensing system, as shown in Fig. 8(b). The ranging precision is measured to be as high as 9.2 μm , which is statistically calculated by the standard deviation out of 120 consecutive measured reflection positions.

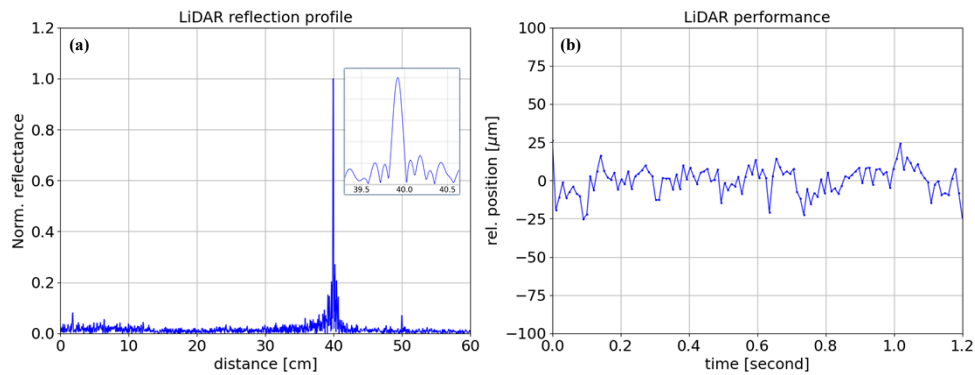


Fig. 8. Measured reflection profile, obtained from the main interferometer.

4. Conclusions

In this paper, the development of an FMCW LiDAR sensing system at 2 μm has been successfully performed based on a hybrid photonic integrated wavelength-tunable laser, and its unmatched performance has been experimentally demonstrated, showing the measured axial resolution of 1.3 cm and range precision of 9.2 μm at 100 Hz measurement rate. According to the results of the thorough characterization of the developed laser, the ambiguity range of the LiDAR will be limited to 13 m in air, which is practically limited by the current architecture of the Vernier filter integrated into the SOI. In general, such an external cavity PIC laser has a large potential to produce a narrow linewidth laser [19,24] in the order of a few kHz linewidth; hence, improving the sensing range. Nevertheless, we believe that our development paves the way towards a fully photonic integrated chip-based FMCW LiDAR at 2 microns, at which most important optical and electro-optic components such as frequency-swept laser, Mach-Zehnder interferometers and photodetectors are all integrated into a single chip. More prominently, we would like to emphasize that the developed LiDAR at 2 microns has inherent advantages of the covert operation, relatively longer propagation length under wet environments and operation in the atmospheric window, so we believe that such a compact FMCW LiDAR system will attract the focus of various research areas such as ranging, metrology and imaging system.

Funding. Eurostars project COLIDE (reference E!114136).

Disclosures. The authors declare no conflicts of interest.

Data availability. Data underlying the results presented in this paper are not publicly available at this time but may be obtained from the authors upon reasonable request.

References

1. M.J. Starek, "Airborne laser terrain mapping," in *Encyclopedia of Estuaries*, Springer: Berlin, Germany (2006).
2. T. Cherian, Y.B. Kumar, and B.S. Reddy, "LiDAR for atmospheric measurements and probing," *Int. J. Eng. Technol.* **5**, 5114–5124 (2012).
3. A.P. Zhevlakov and V.G. Bespalov, "Oil and gas deposits determination by ultraspectral lidar," in *Proc. SPIE, Advanced Environmental, Chemical and Biological Technologies XII*, vol. 9486, 94860 V (2015).
4. U. Weiss and P. Biber, "Plant detection and mapping for agricultural robots using a 3D LiDAR sensor," *Robot. Auton. Syst.* **59**(5), 265–273 (2011).
5. D. Pierrottet, F. Amzajerdian, L. Petway, *et al.*, "Linear FMCW laser radar for precision range and vector velocity measurements," Springer link, Volume 1076: Symposium K – Materials and Devices for Laser Remote Sensing and Optical Communication, 1076-K04-06 (2008).
6. <https://www.electronicsexpress.com/news/business/auto-lidar-set-111-cagr-2020-26-2021-09>.
7. "Silicon photonics: Past, present and future," *Microw. J.* 2019. [online] Available: <https://www.microwavejournal.com/articles/32846-silicon-photonics-past-present-and-future>.
8. P. Munoz, G. Micó, L. A. Bru, *et al.*, "Silicon nitride photonic integration platform for visible, near-infrared and mid-infrared applications," *Sensors* **17**(9), 2088 (2017).

9. L.M. Augustin, R. Santos, E. Haan, *et al.*, “InP-based generic foundry platform for photonic integrated circuit,” *Quantum Electron.* **24**(1), 1–10 (2018).
10. B. J. Isaac, B. Song, S. Pinna, *et al.*, “Indium phosphide photonic integrated circuit transceiver for FMCW LiDAR,” *Quantum Electron.* **25**(6), 1–7 (2019).
11. C. Yu, M. Shangguan, H. Xia, *et al.*, “Fully integrated free-running InGaAs/InP single-photon detector for accurate lidar applications,” *Opt. Express* **25**(13), 14611–14620 (2017).
12. M. Hu, Y. Pang, and L. Gao, “Advances in Silicon-based integrated lidar,” *Sensors* **23**(13), 5920 (2023).
13. R. Wang, A. Malik, I. Simonyte, *et al.*, “Compact GaSb/silicon-on-insulator 2.0 μ m widely tunable external cavity lasers,” *Opt. Express* **24**(25), 28977–28986 (2016).
14. S-P. Ojanen, J. Viheriala, N. Zia, *et al.*, “Widely tunable (2.47–2.64 μ m) hybrid laser based on GaSb/GaInAsSb Quantum-wells and a low-loss Si₃N₄ photonic integrated circuit,” *Laser Photonics Rev.* **17**(7), 2201028 (2023).
15. A. Remis, L. M-Bartolome, M. Paparella, *et al.*, “Unlocking the monolithic integration scenario: optical coupling between GaSb diode lasers epitaxially grown on patterned Si Substrates and passive SiN waveguide,” *Light: Sci. Appl.* **12**(1), 150 (2023).
16. A. Martin, D. Dodane, L. Leviandier, *et al.*, “Photonic integrated circuit-based FMCW coherent LiDAR,” *J. Lightwave Technol.* **36**(19), 4640–4645 (2018).
17. Y. Furukado, H. Abe, Y. Hinakura, *et al.*, “Experimental simulation of ranging action using Si photonic crystal modulator and optical antenna,” *Opt. Express* **26**(14), 18222–18229 (2018).
18. E. Baumann, E.V. Hoenig, E.F. Perez, *et al.*, “Dual-comb spectroscopy with tailored spectral broadening in Si₃N₄ nanophotonics,” *Opt. Express* **27**(8), 11869–11876 (2019).
19. A.V. Lee, Z. Fan, D. Geskus, *et al.*, “Ring resonator enhanced mode-hop-free wavelength tuning of an integrated extended-cavity laser,” *Opt. Express* **28**(4), 5669–5683 (2020).
20. Dennis Derickson, *Fiber Optic Test and Measurement*, (Hewlette-Packard Company, Prentice Hall, 1998).
21. P-H. Merrer, O. Llopis, and G. Cibiel, “Laser stabilization on a fiber ring resonator and application to RF filtering,” *IEEE Photon. Technol. Lett.* **20**(16), 1399–1401 (2008).
22. T-J. Ahn, J.Y. Lee, and D.Y. Kim, “Suppression of nonlinear frequency sweep in an optical frequency-domain reflectometer by use of Hilbert transformation,” *Appl. Opt.* **44**(35), 7630–7634 (2005).
23. T-J. Ahn and D.Y. Kim, “Analysis of nonlinear frequency sweep in high-speed tunable laser sources using a self-homodyne measurement and Hilbert transformation,” *Appl. Opt.* **46**(13), 2394–2400 (2007).
24. C. Xing, W. Jin, O. Terra, *et al.*, “3D integration enables ultralow-noise isolator-free lasers in silicon photonics,” *Nature* **620**(7972), 78–85 (2023).